Toward the Coordination Fingerprint of the Edge-Sharing BO 4 Tetrahedra

Eric Quarez, Eric Gautron, Michael Paris, David Gajan, Jean-Yves Mevellec

Toward the coordination fingerprint of the edge-sharing BO_4 tetrahedra

Eric Quarez,,† Eric Gautron,† Michael Paris,† David Gajan,‡ Jean-Yves Mevellec†*

† Institut des Matériaux Jean Rouxel, IMN, Université de Nantes, CNRS, F-44000 Nantes, France

‡ Very High Field NMR Center, CRMN, Université de Lyon 1, ENS Lyon, CNRS, F-69100 Villeurbanne, France

ABSTRACT: The $K_3Sb_4BO_{13}$ material undergoes an uncommon symmetry increase on cooling, from triclinic symmetry at room temperature to monoclinic symmetry at low temperature. The first-order phase transition is accompanied by the shrinkage of the unit cell resulting in the transformation of every pair of head to tail triangular BO_3 groups into one B_2O_6 unit featuring the unique edge-sharing BO_4 tetrahedra. This is the first material with B_2O_6 units formed through temperature lowering and exhibiting a B-O anionic framework composed uniquely of isolated edge-sharing BO_4 tetrahedra. Several techniques including single crystal XRD experiments, Raman, ^{11}B MAS-NMR spectroscopies and, for the first time, B *K*-edge EELS spectroscopy were

used to evidence the rare and discrete B_2O_6 units. The complete transformation of BO_3 units into B_2O_6 units makes the $K_3Sb_4BO_{13}$ compound the perfect candidate to extract information about B_2O_6 units whose signal can be unambiguously assigned.

INTRODUCTION

Among about 4000 entries of boron-oxygen compounds in ICSD database, only a few of them present a B-O anionic framework containing the rare edge-sharing (es-) BO_4 tetrahedra forming the B_2O_6 units (Fig. 1). At first, the high pressure condition appears to be a key condition to form the B_2O_6 units. Indeed, the majority of borates with (es-) BO_4 tetrahedra, discovered by Huppertz et al., were synthesized at high pressure and high temperature[1–16] with the first one published in 2002.[4] Similarly, α-$Ba_3[B_{10}O_{17}(OH)_2]$ was synthesized at high pressure through hydrothermal reactions at 500 °C and 1000 bar.[17] Unexpectedly, in 2010, the first borate $KZnB_3O_6$ obtained under ambient pressure was prepared[18] showing that high pressure is not mandatory for the formation of (es-) BO_4 tetrahedra. Thereafter, several borates were synthesized under atmospheric environment: $Ba_4Na_2Zn_4(B_3O_6)_2(B_{12}O_{24})$ in 2013[19] and $Li_4Na_2CsB_7O_{14}$[20] and $BaAlBO_4$[21] in 2019. Meanwhile, β-CsB_9O_{14} was obtained under the vacuum-sealed condition.[22] Only twenty-five compounds among thousands of borates were found containing the (es-) BO_4 tetrahedra. The exceptional rarity of this connection mode is explained by the unfavorable formation of the B_2O_6 unit. Indeed, according to Pauling's third rule, the electrostatic repulsion of B···B between two BO_4 tetrahedra is much higher when polyhedra adopt the edge-sharing rather than the corner-sharing connection mode.[23]

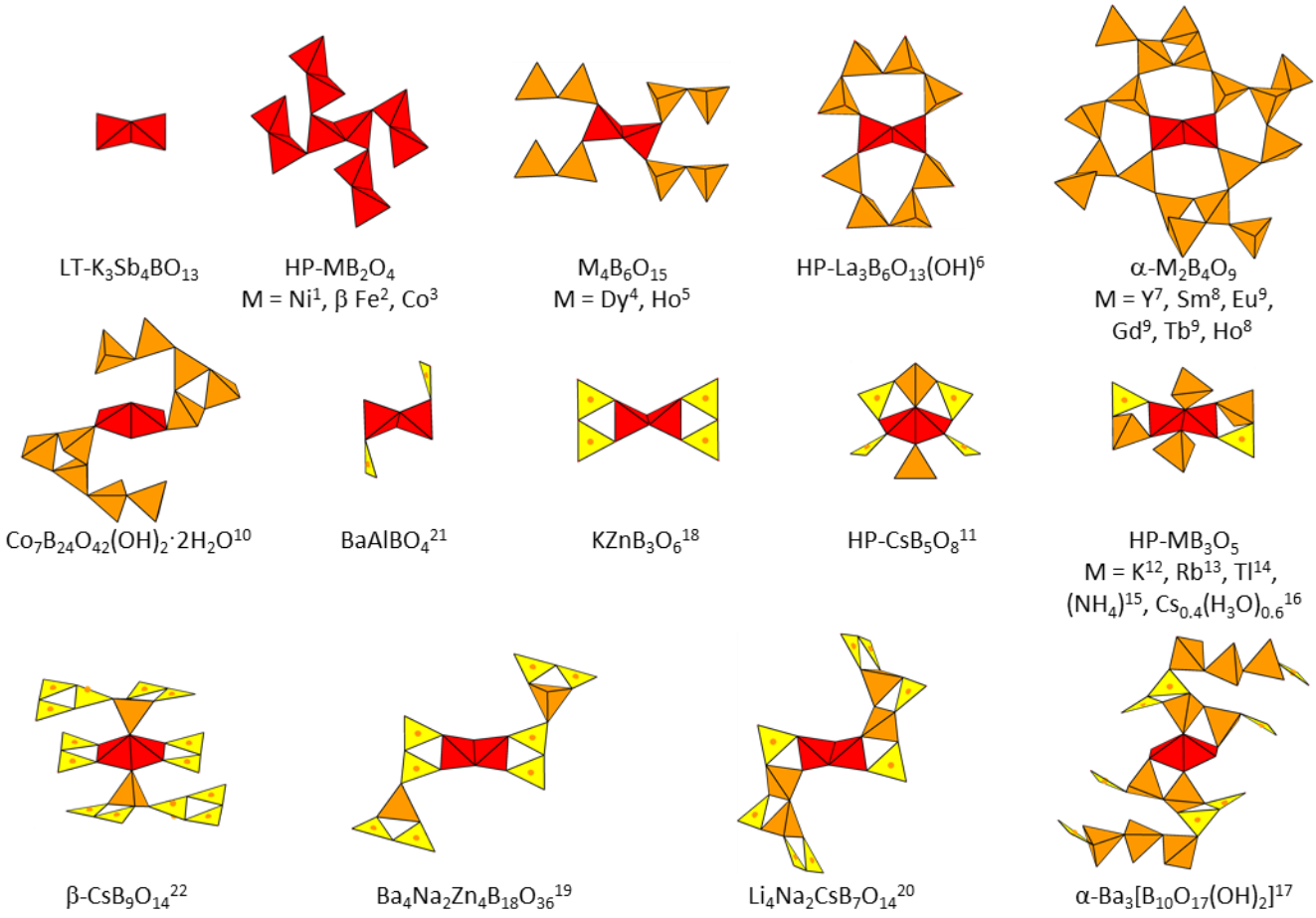

Figure 1. B-O anionic framework of borates containing edge-sharing BO_4 tetrahedra from isolated B_2O_6 unit seen in LT-$K_3Sb_4BO_{13}$ material to the most complex boron framework. B_2O_6 unit is displayed as the central unit of the boron framework. B_2O_6 units, BO_4 tetrahedra and triangular BO_3 groups are represented in red, orange and yellow, respectively.

In the search of new ionic conductor in oxyborates,[24,25] we focus our work on the $K_3Sb_4BO_{13}$ (KSBO) material which adopts the triclinic symmetry at room temperature. Its structure can be described by the stacking of 2D layers of $(Sb_3O_9)_n$ alternatively separated by Sb_2O_{10} dimers and triangular BO_3 groups along the c direction, forming 1D tunnels filled by the mobile K^+ ions (Fig.

2b)[26] that can be replaced, via ion exchange reaction, by the Rb^+ ions.[27] The $K_3Sb_4BO_{13}$ material undergoes an unusual phase transition upon cooling characterized by a symmetry increase, from triclinic *P*-1 space group at room temperature to monoclinic *C*2/*m* space group at low temperature (LT). For phase transitions induced by a change in temperature, the most symmetrical phase is generally the stable phase at high temperature. Indeed, at high temperature the Hamiltonian of a system usually has a higher degree of symmetry. At low temperatures, the appearance of an order normally reduces the symmetry. We observe here the opposite in the case of the KSBO material. Over 2480 phase transitions classified according to symmetry changes, only 10 % correspond to a symmetry increase upon cooling.[28] The phase transition observed in KSBO material is not only uncommon but it is accompanied by the transformation of every pair of head to tail triangular BO_3 groups into one B_2O_6 unit featuring the unique edge-sharing BO_4 tetrahedra (Figure 2). The Figure 1 shows the B-O anionic framework of the borates from the literature containing the B_2O_6 unit. Taking the basic B_2O_6 unit as the central unit, there exists six different nodes to which the B-O blocks can be linked: two nodes from the common edge and four external nodes.[20] The boron framework is varied by replacing the six nodes with different types of B-O blocks. The B-O blocks may be linked to two external nodes ($Co_7B_{24}O_{42}(OH)_2 \cdot 2H_2O$[10] or $BaAlBO_4$[21]), four external nodes (HP-MB_2O_4 M = Ni[1], β Fe[2], Co[3], $M_4B_6O_{15}$ M = Dy[4], Ho[5], HP-$La_3B_6O_{13}(OH)$[6], α-$M_2B_4O_9$ M = Y[7], Sm[8], Eu[9], Gd[9], Tb[9], Ho[8], $KZnB_3O_6$[18], $Ba_4Na_2Zn_4B_{18}O_{36}$[19] and $Li_4Na_2CsB_7O_{14}$[20]) or a combination of two nodes from the common edge and two external nodes (α-$Ba_3[B_{10}O_{17}(OH)_2]$[17]). The case where all the six available nodes are linked to B-O blocks is encountered in HP-CsB_5O_8[11], HP-MB_3O_5 with M = K[12], Rb[13], Tl[14], (NH_4)[15], $Cs_{0.4}(H_3O)_{0.6}$[16] and β-CsB_9O_{14}[22]. The LT-KSBO is the first material presenting the unique structural feature where none B-O block is linked to the B_2O_6 unit. The characterization of this particular isolated B_2O_6 unit is highly important for providing a

specific coordination fingerprint which could be used for example in borate glasses. Consequently, Raman, ^{11}B MAS-NMR and B *K*-edge EELS spectra were used to evidence the isolated B_2O_6 units in the LT-$K_3Sb_4BO_{13}$ material. The spectra are systematically analyzed by comparing them with those obtained above the phase transition temperature featuring the isolated BO_3 units.

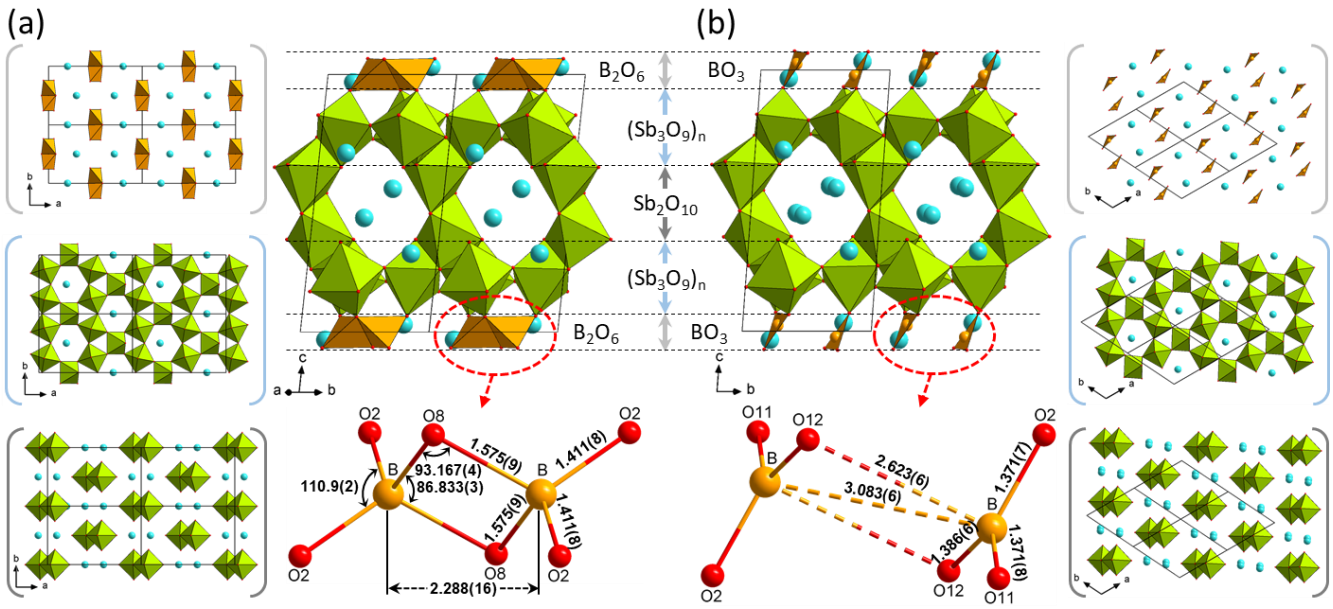

Figure 2. Structures of KSBO material at 200 K, form α (a) and 250 K, form β (b) with layers representation. Bond lengths (Å) and angles (°) in the edge-sharing BO_4 tetrahedra of the α-form and in the pair of head to tail triangular BO_3 groups of the β-form.

EXPERIMENTAL SECTION

Synthesis. Single crystals of the $K_3Sb_4BO_{13}$ compound were grown in platinum crucible in air by slow cooling at 3 °C h^{-1} rate from 1050 to 700 °C and then faster down to room temperature at 300 °C h^{-1} rate. The starting materials K_2CO_3 (Prolabo, 98.0%), Sb_2O_3 (Aldrich, 99.9%) and

$B(OH)_3$ (Merck, 99.8%) were manually ground in a 5 : 2 : 15 ratio. The obtained single crystals were then washed intensively and several times with water to dissolve excess boron products.[27]

X-Ray crystallographic study. Single crystal X-ray diffraction data of $K_3Sb_4BO_{13}$ were collected at T = 200 and 250 K with a Bruker-Nonius Kappa CCD diffractometer using graphite monochromated Mo Kα radiation (λ = 0.71073 Å). Data for the selected crystal were corrected for absorption using JANA2006[29] within the analytical option based on the crystal morphology and optimized with X-SHAPE software.[30] The structures were solved with the ShelXT structure solution program using direct methods and refined with the ShelXL by a full-matrix least-squares technique on F^2 with WinGX interface.[31,32] All atoms were refined with anisotropic thermal parameters except O3 and O7 atoms whose thermal parameters were refined isotropically at T = 200 K. Bond valence sums (BVS) were calculated with JANA2006 using the formula, bond valence = exp((Ro − R)/B), where R is the bond length and Ro and B are tabulated in ref. [33]. Crystal data, data collection and results of the final refinements for the structures at T = 200 and 250 K are listed in Table S1.

Differential Scanning Calorimetry (DSC). DSC measurements of the single crystals (6.8 mg) were performed on a TA instrument (DSC Q20 V24.11 Build 124, New Castle, DE, USA) using cooling and heating rates of 5 K min^{-1}.

Raman spectroscopy. The Raman spectra were recorded from ten single crystals of $K_3Sb_4BO_{13}$ on a micro Raman Renishaw Invia Reflex. The excitation was a 514 nm line of an argon laser with a power on the samples of 15 mW. The grating at 2400 grooves by millimeter provided a spectral

resolution smaller than 3 cm^{-1}. To cool the single crystals, from ambient down to 173 K, the microscope was equipped with a liquid nitrogen cooling stage Linkam Scientific THSM600-PS. All spectra were very similar at T = 173 K (below the phase transition temperature) and at T = 295 K (above the phase transition temperature) demonstrating the reproducibility of the results. One representative spectrum was selected at both temperatures.

Solid-state NMR. ^{11}B Solid State Nuclear Magnetic Resonance (NMR) was carried out on a Bruker Avance III 800 MHz spectrometer using a 3.2 mm LT-MAS DNP probe. Spectra were acquired with a single pulse excitation of 2 μs with a radio-frequency field strength of 30 kHz. MAS speed was 10 kHz. The repetition time was set to 1 s. Spectra were referenced using the signal of an $B(OH)_3$ aqueous solution at 19.6 ppm. The ^{11}B background signal from the probe was removed by subtracting an experimental spectrum of an empty rotor. Spectral fitting was done by using the dmfit freeware.[34]

EELS spectroscopy. Scanning/Transmission Electron Microscopy (S/TEM) experiments were performed on a probe corrected Themis Z G3 (Thermo Fisher Scientific). Electron Energy Loss (EELS) spectra were obtained with a GIF Quantum ERS 966 imaging filter (Gatan) equipped with an additional direct electron detection camera K2 Summit (Gatan) that can be inserted in front of the classical CCD camera. The amount of boron in the material is quite low (< 5 % at.). The K2 camera was therefore used in counting mode to obtain a high signal to noise ratio and the spectra were acquired at a low dispersion (0.5 eV/channel) to get intense enough B *K*-edge while maintaining energy resolution (1 eV for zero-loss FWHM).

Around twenty crystals were selected with a binocular before being gently crushed in ethanol in an agate mortar. A drop of this solution was then deposited on a copper grid covered with a thin holey carbon film. A cryo sample holder (Model 2550, Fischione) was used to characterize the sample first at ambient temperature and then at low temperature (96 K). Energy dispersive X-ray (EDX) analysis confirms the composition of the single crystals (Figure S1). EELS spectra were acquired in STEM mode under these conditions: 300 kV accelerating voltage, 100 pA beam current, 30 mrad convergence semi-angle, 70 mrad collection semi-angle. The spectra were integrated on spectrum images area. A power law was used to subtract the background; plural scattering was not removed. Pixel size and dwell times were chosen to have enough signal while limiting the radiation damage that can induce the degradation of BO_4 groups into BO_3 groups.[35,36]

RESULT AND DISCUSSION

Thermal analyses and X-ray diffraction study. Single crystals of the KSBO material were synthetized by flux crystal growth.[27] The compound at room temperature crystallizes in the triclinic system with centrosymmetric space group *P*-1.[26] The occurrence of a thermal phase transition in KSBO was confirmed by differential scanning calorimetry (DSC) measurements (Fig. 3). The DSC curves for the single crystals exhibit a single exothermic peak at 194 K during the cooling process. This peak corresponds to the transition to the low-temperature phase. In contrast, the DSC traces of KSBO exhibit an endothermic peak at 210 K during the heating process. The relatively large thermal hysteresis of ca. 16 K and the distinct peak indicate a first-order phase transition. The crystal analyses of KSBO were performed at 200 K (low-temperature phase called form α) and at 250 K (high temperature phase called form β). The compound at 200 K crystallizes in a monoclinic space group *C*2/*m* indicating a symmetry increase in comparison with the room temperature

structure,[26,27] with unit cell parameters of a = 12.2032(5) Å, b = 7.4881(6) Å, c = 13.0698(19) Å and β = 101.636(6)°. When the temperature was increased, a structural phase change occurred (Figure S2, Table S2). The crystal structure at 250 K shows that KSBO crystallizes in the same *P*-1 space group as that at 295 K[27] but with slightly different unit cell parameters. The cell parameters at 250 K are a = 7.1168(8) Å, b = 7.2114(10) Å, c = 13.2218(7) Å, α = 81.923(7)°, β = 99.760(7)° et γ = 117.098(12)°. Note that further data collections at 200 K and again at 250 K on the same single crystal give, respectively, the monoclinic and triclinic structures, confirming the reversibility of the phase transition. The structures of the low and high temperature phases are very similar with 2D layers of $(Sb_3O_9)_n$ alternatively separated by Sb_2O_{10} dimers and B-O blocks along the c direction, forming 1D tunnels filled by the K^+ ions (Figure 2). There are two noticeable differences. First, the potassium sites of the high temperature phase located in the layer of the Sb_2O_{10} dimers are split, as observed for the room temperature structure.[27] This is related to the mobility of the K^+ ions in the 1D tunnels formed by the SbO_6 octahedra. By decreasing the temperature, the mobility of the K^+ ions is reduced and consequently, the sites are not split anymore. Secondly and more importantly, the B-O blocks are altered from high to low temperature phase. Indeed, each pair of head to tail triangular BO_3 groups is transformed into one B_2O_6 unit featuring the unique (-es) BO_4 tetrahedra. In contrast to previously reported ambient and high pressure borates, because the B_2O_6 unit is located on a centre of inversion (2/*m* site symmetry), both B-O bond lengths inside the B_2O_2 ring, as well as both B-O bond lengths outside the ring, are equal (Figures 2 and S3). The geometry of the (-es) BO_4 tetrahedra is nonetheless consistent with other borates containing the same structural motif. As a common feature, the like-charges repulsion will push the positively charged B^{3+} cations apart in the (-es) polyhedra to minimize the electrostatic potential. Thus, the B–O bond lengths inside the B_2O_2 ring (B-O = 1.575(9) Å) are larger than those outside the B_2O_2 ring (B-O

= 1.411(8) Å), the average B-O bond length of 1.493 Å being slightly higher than the averaged bond length of a BO_4 tetrahedron (1.476 Å).[37] In parallel, the O-B-O angle within the B_2O_2 ring is remarkably reduced 86.833(3)° compared to the ideal value of 109.48°. The O-B-O bond angle outside the B_2O_2 ring is close to the ideal value, about 110.9(2)°. The considerable shrinkage of the O-B-O angle within the planar B_2O_2 ring is the factor most responsible for the significant expansion of the B···B interatomic distances. Indeed, the B···B bond length inside the (-es) tetrahedra of LT-KSBO is 2.288(16) Å which is the largest value found in the borates containing this structural motif (Fig. S2). Bond-valence sum (BVS) calculation confirms that all the atoms in the compound, at low and high temperature, adopted normal valence states (Figure S4, Table S3).

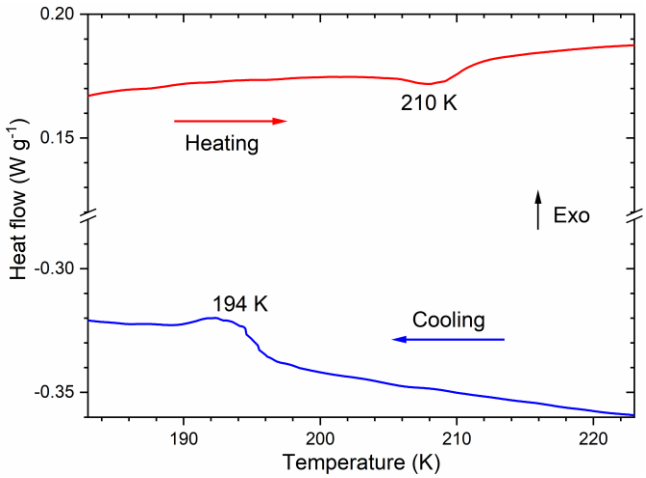

Figure 3. DSC curves of KSBO recorded at the rate of 5 K min^{-1} during a cooling–heating (blue-red lines) cycle.

To investigate the structural change in detail and, in particular, to better understand the transformation of (-es) BO_4 tetrahedra into a pair of head to tail planar BO_3 triangles, we study the structural distortions implied by the phase transition from *C*2/*m* to *P*-1 space group using AMPLIMODES, a computer program available on the Bilbao Crystallographic Server.[38,39] The analysis consists in decomposing the symmetry-breaking distortion present in the distorted

structure into contributions from different symmetry-adapted modes. Given the high- and the low-symmetry structures, AMPLIMODES determines the atomic displacements that relate them, defines a basis of symmetry-adapted modes, and calculates the amplitudes and polarization vectors of the distortion modes of different symmetry frozen in the structure. The mode decomposition applied to the phase transition of KSBO gives two different modes, GM1+ and GM2+ with an amplitude of 0.9313 and 1.0604 Å, respectively (Tables S3-S6). Surprisingly, the primary mode, GM2+, has an amplitude only slightly higher than the secondary mode GM1+. The Figure 4 represents the polarization vectors of GM1+ and GM2+ modes (see also animated Figure S5). In the GM2+ distortion, the magnitude of the displacement of B and O12 atoms is much larger than that of all other atoms. B atoms are pushed back from each other, moving towards the triangles formed by O2, O11 and O12 atoms. O12 atoms of the common edge move along a+b and -a-b directions so as to separate both triangles from each other. These movements are clearly related to the transformation of the B_2O_6 unit into a pair of triangular BO_3 groups. In order to accompany the transformation, nearby octahedra rotate with a smaller magnitude. In the GM1+ distortion, the B atoms displace in the (ab) plane in order to move away from each other. All oxygen atoms of the B_2O_6 unit are also repelled from their symmetric counterpart in order to slightly enlarge the triangles and to move them away from each other. As for the GM2+ distortion, the displacements of the oxygen atoms of nearby octahedra have a much smaller magnitude. These results provide a clear view of the moving mechanisms relative to the deconstruction and the reorganization of the B_2O_6 unit into two planar BO_3 triangles. The volume of the triclinic cell at T = 250 K (V = 593.79 $Å^3$) is higher, as expected, than the volume of the monoclinic cell at T = 200 K in the triclinic setting (V_{tric} = 584.88 $Å^3$). The lattice expansion, associated with the temperature increase (Figure S6), widens the interatomic distances, in particular the distances between neighbor B atoms and

O12 atoms of the common edge, and results concurrently in the phase transition and the transformation of a B_2O_6 unit into two BO_3 units.

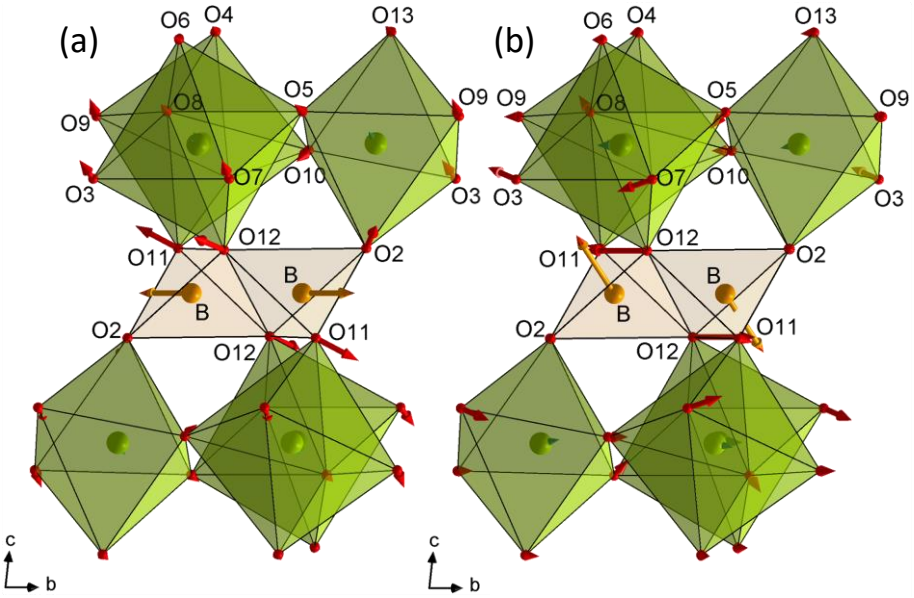

Figure 4. Polarization vector of the distortions corresponding to the modes GM1+ (a) and GM2+ (b) in KSBO. The scale of the displacement vectors has been enlarged. Potassium atoms are omitted.

Raman spectroscopy. The Figure 5 shows the Raman spectra of the KSBO single crystals above (295 K) and below the phase transition temperature (173 K). Although the wavenumbers were scanned up to 4000 cm^{-1}, no Raman band was recorded above 1300 cm^{-1}. Below 850 cm^{-1}, bands of complex bending and stretching vibrations of the lattice, including the metal ions, are visible. There are clearly some similarities between both spectra which originate from the close structural relationship. In contrast to the region below 850 cm^{-1}, the regions above 850 cm^{-1} is particularly modified due to the phase transition resulting in the transformation of two BO_3 groups into one B_2O_6 unit. Indeed, the bands in the range 900-1300 cm^{-1} (inset Fig. 5), because of the atomic masses

of the different elements in the $K_3Sb_4BO_{13}$ material, can only correspond to modes involving the stretching of B-O bonds. Depending on the oxygen coordination of boron, wavenumbers are expected between 850 and 1100 cm^{-1} for BO_4 groups[40,41] and between 1200 and 1450 cm^{-1} for BO_3 groups[41,42]. Since the structures above and below the phase transition temperature exhibit only isolated BO_3 and B_2O_6 groups, respectively, at high temperature, the Raman bands, denoted at 1004, 1218 and 1244 cm^{-1}, could be assigned to the BO_3 groups while, at low temperature, the Raman bands, denoted at 960, 1069, 1090 and 1107 cm^{-1}, could be assigned to the B_2O_6 units. In the HP-borates studied by Huppertz et al., two Raman-active ranges (1253−1271 and 1431−1444 cm^{-1}) have been assigned to modes of edge-sharing BO_4 tetrahedra.[43] No such Raman-active modes at the corresponding wavelengths could be detected in LT-KSBO. Raman bands attribution is strongly dependent upon the structure and the interconnecting metal cations. However, Raman spectra for LT and RT-KSBO confirm well that both the BO_4 and BO_3 groups are present in the compound depending on the temperature.

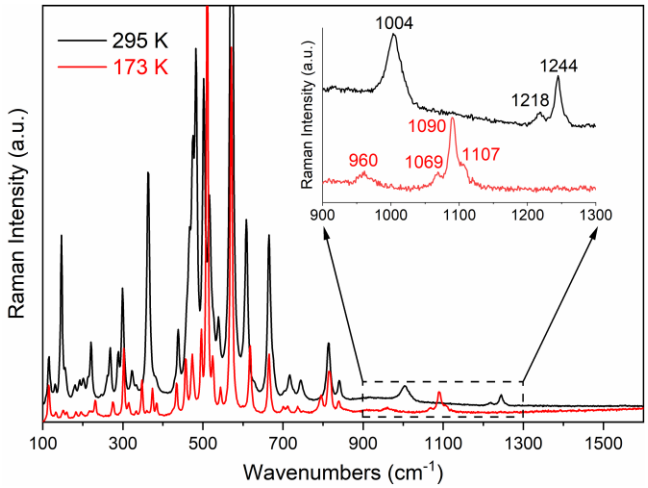

Figure 5. Raman spectra of KSBO single crystals at 173 and 295 K in the range of 100–1600 cm^{-1}.

Solid-state NMR. The ^{11}B MAS NMR spectrum of KSBO acquired at room temperature reveals a single site (Figure 6). The isotropic chemical shift is 16.7 ppm, the quadrupolar coupling constant C_Q is 2.6 MHz and the asymmetry parameter η for quadrupolar is 0. Such values are typical for BO_3 units.[44] From 220K to 180K, the BO_3 line progressively vanishes whereas a new line grows at lower frequency. In accordance with transition temperature of KSBO, this new line is attributed to B_2O_6 units. Note that because of the shrinkage of the unit cell, the isotropic chemical shift depends on the temperature. Thus, the BO_3 line shifts from 16.7 ppm at 298K to 15.7 ppm at 200K. The B_2O_6 line shifts from 1.3 ppm at 200 K to 2.0 ppm at 100 K as well. This agrees well with the 1.75 and 2.4 ppm values previously reported for HP- KB_3O_5 and $KZnB_3O_6$, respectively.[12] At 100 K, the shape of the B_2O_6 line does not present any effect of second-order quadrupolar interaction. On the contrary, it can be adequately fitted with a single Lorentzian line with 1.0 ppm of full width at half maximum. This suggests a low quadrupolar coupling constant. By using the SATRAS method,[45] we estimated the quadrupolar product ($C_{Q\eta} = C_Q\sqrt{1 + {\eta^2}/{3}}$ with $0 \leq \eta \leq 1$) to be 320 kHz. This value agrees well with the value below 500 kHz reported for $La_3B_6O_{13}(OH)$[6] but is lower than the 1.2 and 0.8 MHz values reported for HP- KB_3O_5 and $KZnB_3O_6$, respectively.[12] For KSBO, the low value of the quadrupolar product does not reflect the strong distortion of the BO_4 tetrahedra. One possible explanation could be related to the specific position of the B_2O_6 unit located on a centre of inversion. Moreover, because the quadrupolar product is too low to explain the linewidth of the B_2O_6 unit, we associate the width with a distribution of isotropic chemical shift due to a gradient of temperature within the sample. The present ^{11}B NMR data agree reasonably well with those of previous studies,[6,12] and allows in the case of KSBO, where there exist only B_2O_6 units depending on the temperature, the unambiguous assignment of the B_2O_6 signal.

However, further works are needed to allow corner- and edge-sharing BO_4 tetrahedra to be clearly discriminated by ^{11}B NMR.

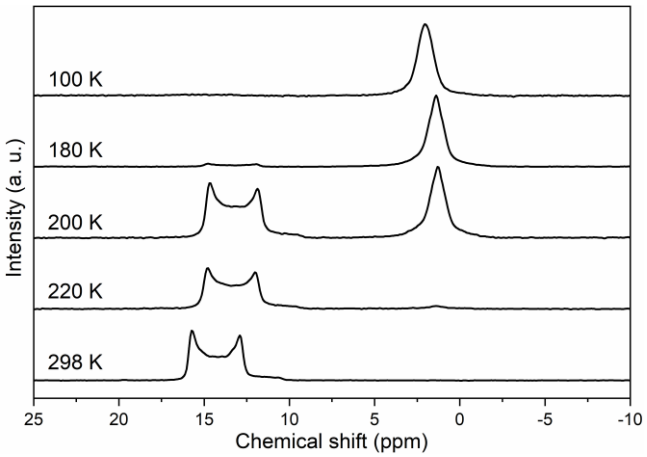

Figure 6. ^{11}B MAS NMR spectra of KSBO at various temperatures.

EELS spectroscopy. Boron *K*-edge EELS spectra of KSBO compound are given in Figure 7. At room temperature, the B *K*-edge of KSBO presents two main features common in borates containing BO_3 groups: an initial intense peak (peak A) followed by a broader peak.[35,36,46] The peak A, around 193.2 eV, is assigned to a transition of B 1*s* to $2p_z$ (π*) orbital. The broad peak C, centered 10 eV higher in energy, is assigned to transitions of B 1*s* electrons to unoccupied B-O sigma antibonding (σ*) orbitals of *e*' symmetry. The weak peak B (around 197.5 eV) arises from a dipole-forbidden transition from B 1*s* → a_1' (σ*) states but weakly allowed by distortion.

For phases containing regular BO_4 groups with small angular and bond variations from an ideal tetrahedron, the B *K*-edge EELS spectrum exhibits mainly two bands B and C.[35,36,46] The band B is assigned to transitions of B 1*s* electrons to unoccupied sigma antibonding (σ*) states of t_2 symmetry (peak around 198 eV) and a_1 symmetry (weaker peak at 200 eV). The band C (around 203 eV) is assigned to transitions of B 1*s* electrons to the unoccupied σ* orbitals of a_1 and t_2

symmetry.[35,36,46] The spectrum at low temperature (96 K) of KSBO exhibits one peak A and two bands B and C (Figure 7). The peak A is caused by electron-beam damage during data acquisition involving conversion of part of BO_4 to BO_3 groups.[35,36,46] In contrast to B *K*-edge EELS spectra of borates containing regular tetrahedra, the band B of LT-KSBO exhibits a distinct peak at ca. 196.7 eV below this usually found at ca. 198 eV and a peak similarly intense at ca. 200.2 eV. This results from the highly distorted BO_4 tetrahedra containing two short (2 x 1.411 Å) and two long B-O distances (2 x 1.575 Å) with B-site symmetry C_2. The distortion causes the loss of degeneracy of the σ* (t_2) orbital and peak broadening.[36,46,47] Because σ* antibonding levels for long bonds are expected to be closer to the bottom of the conduction band than σ* antibonding levels for short bonds,[47] the peak at ca. 196.7 eV could be assigned to the longest B-O distance in the BO_4 tetrahedron and the peak at ca. 200.2 eV could be assigned to the 1.411 Å distance. Highly distorted tetrahedra are generally obtained in borates containing B_2O_6 units due to the repulsion of boron atoms which deviate the O-B-O angles from the ideal value, increases B-O bond lengths inside the B_2O_2 ring and decreases those outside the B_2O_2 ring (Figure S3). One can expect to obtain similar B *K*-edge EELS spectra for other borates containing B_2O_6 units to that obtained for LT-KSBO. Due to the particularity of the distorted tetrahedra composing the B_2O_6 units, the presence of a broad intense B band in the B *K*-edge EELS spectrum is a motive to investigate the existence of this rare structural motif.

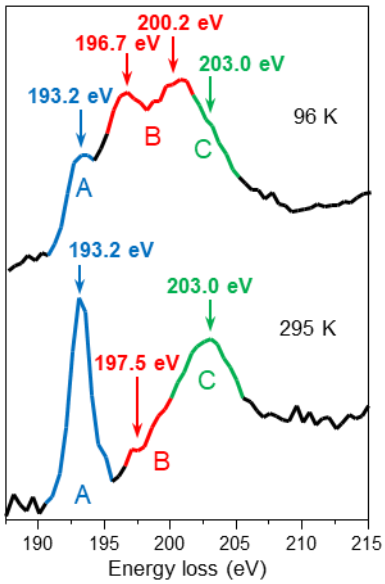

Figure 7. Experimental EELS B *K*-edge spectra for KSBO at 96 and 295 K.

CONCLUSION

$K_3Sb_4BO_{13}$ undergoes a reversible phase transition with the formation, at low temperature, of the isolated edge-sharing BO_4 tetrahedra. The temperature lowering involves a lattice compression which, in particular, shortens the B···B and B···O distances of each pair of planar BO_3 triangles units and leads to the formation of B_2O_6 units. In the search of a specific fingerprint of the B_2O_6 unit using different techniques such as Raman, ^{11}B NMR and B *K*-edge EELS spectroscopies, it appears that the latter could be used to evidence the B_2O_6 units. Despite the fact that B *K*-edge EELS is not suitable to provide a specific fingerprint of the B_2O_6 unit, it could provide a characteristic signal of the distorted tetrahedra forming the B_2O_6 unit, which is the common feature shared by borates containing this special structural motif.

ASSOCIATED CONTENT

Supporting Information

The Supporting Information is available free of charge on the ACS Publications website at DOI: *** (PDF).

Crystal data, data collection and structure refinement parameters (Table S1), single crystal composition (Figure S1), geometric relationship between monoclinic and triclinic cells (Figure S2), matrices and equations of the cell transformation (Table S2), interatomic distances and angles in the B_2O_6 units of borates containing edge-sharing BO_4 tetrahedra (Figure S3), structural representation with atom labelling (Figure S4), atom pairings of monoclinic and triclinic structures (Table S3), mode decomposition and polarization vectors of the distortion components (Tables S4-S6), animation of the distortion modes (Figure S5), thermal expansivity indicatrix (Figure S6).

Accession Codes

CSD 1962261-1962262 contain the supplementary crystallographic data for this paper. These data can be obtained free of charge via www.ccdc.cam.ac.uk/data_request/cif, or by emailing data_request@ccdc.cam.ac.uk, or by contacting The Cambridge Crystallographic Data Centre, 12 Union Road, Cambridge CB2 1EZ, UK; fax: +44 1223 336033.

AUTHOR INFORMATION

Corresponding Author

E-mail: eric.quarez@cnrs-imn.fr

Notes

The authors declare no competing financial interest.

ACKNOWLEDGMENT

The authors would like to thank Pr. P. Moreau (IMN) for fruitful comments as well as L. Cournede and S. Grolleau (IMN) for complementary computations and thermal analyses. Funded by the French Contrat Plan État-Région and the European Regional Development Fund of Pays de la Loire, the CIMEN Electron Microscopy Center in Nantes is greatly acknowledged. Financial support from the IR-RMN-THC Fr3050 CNRS for conducting the research is gratefully acknowledged.

References

(1) Knyrim, J. S.; Roeßner, F.; Jakob, S.; Johrendt, D.; Kinski, I.; Glaum, R.; Huppertz, H. Formation of Edge-Sharing BO4 Tetrahedra in the High-Pressure Borate HP-NiB2O4. *Angewandte Chemie International Edition* **2007**, *46* (47), 9097–9100. https://doi.org/10.1002/anie.200703399.

(2) Neumair, S. C.; Glaum, R.; Huppertz, H. Synthesis and Crystal Structure of the High-Pressure Iron Borate β-FeB2O4. *Zeitschrift für Naturforschung B* **2009**, *64* (8), 883–890. https://doi.org/10.1515/znb-2009-0802.

(3) Neumair, S. C.; Kaindl, R.; Huppertz, H. Synthesis and Crystal Structure of the High-Pressure Cobalt Borate HP-CoB2O4. *Zeitschrift für Naturforschung B* **2010**, *65* (11), 1311–1317. https://doi.org/10.1515/znb-2010-1104.

(4) Huppertz, H.; von der Eltz, B. Multianvil High-Pressure Synthesis of Dy4B6O15: The First Oxoborate with Edge-Sharing BO4 Tetrahedra. *J. Am. Chem. Soc.* **2002**, *124* (32), 9376–9377. https://doi.org/10.1021/ja017691z.

(5) Huppertz, H. High-Pressure Preparation, Crystal Structure, and Properties of RE4B6O15 (RE = Dy, Ho) with an Extension of the "Fundamental Building Block"-Descriptors. *Zeitschrift für Naturforschung B* **2014**, *58* (4), 278–290. https://doi.org/10.1515/znb-2003-0406.

(6) Fuchs, B.; Heymann, G.; Wang, X.; Tudi, A.; Bayarjargal, L.; Siegel, R.; Schmutzler, A.; Senker, J.; Joachim-Mrosko, B.; Saxer, A.; Yang, Z.; Pan, S.; Huppertz, H. La3B6O13(OH): The First Acentric High-Pressure Borate Displaying Edge-Sharing BO4 Tetrahedra. *Chemistry – A European Journal* **2020**, *26* (30), 6851–6861. https://doi.org/10.1002/chem.201905419.

(7) Schmitt, M. K.; Huppertz, H. High-Pressure Synthesis and Crystal Structure of α-Y2B4O9. *Zeitschrift für Naturforschung B* **2017**, *72* (12), 977–982. https://doi.org/10.1515/znb-2017-0150.
(8) Emme, H.; Huppertz, H. High-Pressure Syntheses of α-RE2B4O9 (RE = Sm, Ho), with a Structure Type Displaying Edge-Sharing BO4 Tetrahedra. *Acta Cryst C* **2005**, *61* (3), i29–i31. https://doi.org/10.1107/S0108270104030446.
(9) Emme, H.; Huppertz, H. High-Pressure Preparation, Crystal Structure, and Properties of α-(RE)2B4O9 (RE=Eu, Gd, Tb, Dy): Oxoborates Displaying a New Type of Structure with Edge-Sharing BO4 Tetrahedra. *Chemistry – A European Journal* **2003**, *9* (15), 3623–3633. https://doi.org/10.1002/chem.200204696.
(10) Neumair, S. C.; Kaindl, R.; Huppertz, H. The New High-Pressure Borate Co7B24O42(OH)2·2H2O—Formation of Edge-Sharing BO4 Tetrahedra in a Hydrated Borate. *Journal of Solid State Chemistry* **2012**, *185*, 1–9. https://doi.org/10.1016/j.jssc.2011.10.028.
(11) Sohr, G.; Többens, D. M.; Schmedt auf der Günne, J.; Huppertz, H. HP-CsB5O8: Synthesis and Characterization of an Outstanding Borate Exhibiting the Simultaneous Linkage of All Structural Units of Borates. *Chemistry – A European Journal* **2014**, *20* (51), 17059–17067. https://doi.org/10.1002/chem.201404018.
(12) Neumair, S. C.; Vanicek, S.; Kaindl, R.; Többens, D. M.; Martineau, C.; Taulelle, F.; Senker, J.; Huppertz, H. HP-KB3O5 Highlights the Structural Diversity of Borates: Corner-Sharing BO3/BO4 Groups in Combination with Edge-Sharing BO4 Tetrahedra. *European Journal of Inorganic Chemistry* **2011**, *2011* (27), 4147–4152. https://doi.org/10.1002/ejic.201100618.
(13) Sohr, G.; Neumair, S. C.; Huppertz, H. High-Pressure Synthesis and Characterization of the Alkali Metal Borate HP-RbB3O5. *Zeitschrift für Naturforschung B* **2012**, *67* (11), 1197–1204. https://doi.org/10.5560/znb.2012-0248.
(14) Sohr, G.; Perfler, L.; Huppertz, H. The High-Pressure Thallium Triborate HP-TlB3O5. *Zeitschrift für Naturforschung B* **2014**, *69* (11–12), 1260–1268. https://doi.org/10.5560/znb.2014-4124.
(15) Sohr, G.; Wilhelm, D.; Vitzthum, D.; Schmitt, M. K.; Huppertz, H. The High-Pressure Borate HP-(NH4)B3O5. *Zeitschrift für anorganische und allgemeine Chemie* **2014**, *640* (14), 2753–2758. https://doi.org/10.1002/zaac.201400312.
(16) Sohr, G.; Neumair, S. C.; Heymann, G.; Wurst, K.; Schmedt auf der Günne, J.; Huppertz, H. Oxonium Ions Substituting Cesium Ions in the Structure of the New High-Pressure Borate HP-Cs1−x(H3O)XB3O5 (X=0.5–0.7). *Chemistry – A European Journal* **2014**, *20* (15), 4316–4323. https://doi.org/10.1002/chem.201303550.
(17) Jen, I.-H.; Lee, Y.-C.; Tsai, C.-E.; Lii, K.-H. Edge-Sharing BO4 Tetrahedra in the Structure of Hydrothermally Synthesized Barium Borate: α-Ba3[B10O17(OH)2]. *Inorg. Chem.* **2019**, *58* (7), 4085–4088. https://doi.org/10.1021/acs.inorgchem.9b00345.
(18) Jin, S.; Cai, G.; Wang, W.; He, M.; Wang, S.; Chen, X. Stable Oxoborate with Edge-Sharing BO4 Tetrahedra Synthesized under Ambient Pressure. *Angewandte Chemie International Edition* **2010**, *49* (29), 4967–4970. https://doi.org/10.1002/anie.200907075.
(19) Chen, X.; Chen, Y.; Sun, C.; Chang, X.; Xiao, W. Synthesis, Crystal Structure, Spectrum Properties, and Electronic Structure of a New Three-Borate Ba4Na2Zn4(B3O6)2(B12O24) with Two Isolated Types of Blocks: 3[3Δ] and 3[2Δ+1T]. *Journal of Alloys and Compounds* **2013**, *568*, 60–67. https://doi.org/10.1016/j.jallcom.2013.03.103.

(20) Mutailipu, M.; Zhang, M.; Li, H.; Fan, X.; Yang, Z.; Jin, S.; Wang, G.; Pan, S. Li 4 Na 2 CsB 7 O 14 : A New Edge-Sharing [BO 4] 5− Tetrahedra Containing Borate with High Anisotropic Thermal Expansion. *Chemical Communications* **2019**, *55* (9), 1295–1298. https://doi.org/10.1039/C8CC09422E.
(21) Guo, F.; Han, J.; Cheng, S.; Yu, S.; Yang, Z.; Pan, S. Transformation of the B–O Units from Corner-Sharing to Edge-Sharing Linkages in BaMBO4 (M = Ga, Al). *Inorg. Chem.* **2019**, *58* (12), 8237–8244. https://doi.org/10.1021/acs.inorgchem.9b01157.
(22) Han, S.; Huang, C.; Tudi, A.; Hu, S.; Yang, Z.; Pan, S. β-CsB9O14: A Triple-Layered Borate with Edge-Sharing BO4 Tetrahedra Exhibiting a Short Cutoff Edge and a Large Birefringence. *Chemistry – A European Journal* **2019**, *25* (50), 11614–11619. https://doi.org/10.1002/chem.201902527.
(23) Burdett, J. K.; McLarnan, T. J. An Orbital Explanation for Pauling's Third Rule. *J. Am. Chem. Soc.* **1982**, *104* (19), 5229–5230. https://doi.org/10.1021/ja00383a041.
(24) Doux, J.-M.; Hoang, K.; Joubert, O.; Quarez, E. Oxygen Ion Transport and Effects of Doping in $Ba_3Ti_3O_6(BO_3)_2$. *Chemistry of Materials* **2017**, *29* (15), 6425–6433. https://doi.org/10.1021/acs.chemmater.7b01831.
(25) Doux, J.-M.; Hoang, K.; Joubert, O.; Hamon, J.; Massuyeau, F.; Quarez, E. Ionic to Electronic Transport in $Ba_3Ti_3O_6(BO_3)_2$ under Reducing Atmosphere. *ACS Applied Energy Materials* **2018**, *1* (2), 510–521. https://doi.org/10.1021/acsaem.7b00124.
(26) Doux, J.-M.; Leguay, L.; Le Gal La Salle, A.; Joubert, O.; Quarez, E. K3Sb4O10(BO3): A Solid State K-Ion Conductor. *Solid State Ionics* **2018**, *324*, 260–266. https://doi.org/10.1016/j.ssi.2018.07.018.
(27) Doux, J.-M.; Stephant, N.; Salle, A. L. G. L.; Joubert, O.; Guyomard, D.; Quarez, E. New KRb2Sb4BO13 and Rb3Sb4BO13 Compounds Prepared by Rb+/K+ Ion Exchange from the K3Sb4BO13 Ion Conductor. *CrystEngComm* **2019**, *21* (4), 594–601. https://doi.org/10.1039/C8CE01712C.
(28) Tomaszewski, P. E. Structural Phase Transitions in Crystals. II. Statistical Analysis. *Phase Transitions* **1992**, *38* (3), 221–228. https://doi.org/10.1080/01411599208222900.
(29) Petříček, V.; Dušek, M.; Palatinus, L. Crystallographic Computing System JANA2006: General Features. *Zeitschrift für Kristallographie - Crystalline Materials* **2014**, *229* (5), 345–352. https://doi.org/10.1515/zkri-2014-1737.
(30) *Stoe & Cie, X-SHAPE, Stoe & Cie, Darmstadt, Germany*; 1998.
(31) Sheldrick, G. M. SHELXT - Integrated Space-Group and Crystal-Structure Determination. *Acta Crystallogr A Found Adv* **2015**, *71* (Pt 1), 3–8. https://doi.org/10.1107/S2053273314026370.
(32) Farrugia, L. J. WinGX and ORTEP for Windows: An Update. *J Appl Cryst* **2012**, *45* (4), 849–854. https://doi.org/10.1107/S0021889812029111.
(33) Gagné, O. C.; Hawthorne, F. C. Comprehensive Derivation of Bond-Valence Parameters for Ion Pairs Involving Oxygen. *Acta Crystallogr B Struct Sci Cryst Eng Mater* **2015**, *71* (Pt 5), 562–578. https://doi.org/10.1107/S2052520615016297.
(34) Massiot, D.; Fayon, F.; Capron, M.; King, I.; Calvé, S. L.; Alonso, B.; Durand, J.-O.; Bujoli, B.; Gan, Z.; Hoatson, G. Modelling One- and Two-Dimensional Solid-State NMR Spectra. *Magnetic Resonance in Chemistry* **2002**, *40* (1), 70–76. https://doi.org/10.1002/mrc.984.
(35) Sauer, H.; Brydson, R.; Rowley, P. N.; Engel, W.; Thomas, J. M. Determination of Coordinations and Coordination-Specific Site Occupancies by Electron Energy-Loss

Spectroscopy: An Investigation of Boron—Oxygen Compounds. *Ultramicroscopy* **1993**, *49* (1), 198–209. https://doi.org/10.1016/0304-3991(93)90226-N.
(36) Garvie, L. A. J.; Craven, A. J.; Brydson, R. Parallel Electron Energy-Loss Spectroscopy (PEELS) Study of B in Minerals: The Electron Energy-Loss near-Edge Structure (ELNES) of the B K Edge. *American Mineralogist* **1995**, *80* (11–12), 1132–1144. https://doi.org/10.2138/am-1995-11-1204.
(37) Zobetz, E. Geometrische Größen Und Einfache Modellrechnungen Für BO4-Gruppen. *Zeitschrift für Kristallographie* **1990**, *191* (1–2), 45–57. https://doi.org/10.1524/zkri.1990.191.1-2.45.
(38) Orobengoa, D.; Capillas, C.; Aroyo, M. I.; Perez-Mato, J. M. AMPLIMODES: Symmetry-Mode Analysis on the Bilbao Crystallographic Server. *J Appl Cryst* **2009**, *42* (5), 820–833. https://doi.org/10.1107/S0021889809028064.
(39) Perez-Mato, J. M.; Orobengoa, D.; Aroyo, M. I. Mode Crystallography of Distorted Structures. *Acta Cryst A* **2010**, *66* (5), 558–590. https://doi.org/10.1107/S0108767310016247.
(40) Laperches, J. P.; Tarte, P. Spectres d'absorption Infrarouge de Borates de Terres Rares. *Spectrochimica Acta* **1966**, *22* (7), 1201–1210. https://doi.org/10.1016/0371-1951(66)80023-1.
(41) Ren, M.; Lin, J. H.; Dong, Y.; Yang, L. Q.; Su, M. Z.; You, L. P. Structure and Phase Transition of GdBO3. *Chem. Mater.* **1999**, *11* (6), 1576–1580. https://doi.org/10.1021/cm990022o.
(42) Steele, W. C.; Decius, J. C. Infrared Absorption of Lanthanum, Scandium, and Indium Borate and the Force Constants of Borate Ion. *J. Chem. Phys.* **1956**, *25* (6), 1184–1188. https://doi.org/10.1063/1.1743175.
(43) Neumair, S. C.; Knyrim, J. S.; Oeckler, O.; Glaum, R.; Kaindl, R.; Stalder, R.; Huppertz, H. Intermediate States on the Way to Edge-Sharing BO4 Tetrahedra in M6B22O39·H2O (M=Fe, Co). *Chemistry – A European Journal* **2010**, *16* (46), 13659–13670. https://doi.org/10.1002/chem.201001611.
(44) Multinuclear Solid-State Nuclear Magnetic Resonance of Inorganic Materials, Volume 6 - 1st Edition https://www.elsevier.com/books/multinuclear-solid-state-nuclear-magnetic-resonance-of-inorganic-materials/mackenzie/978-0-08-043787-3 (accessed Oct 5, 2020).
(45) Skibsted, J.; Nielsen, N. C.; Bildsøe, H.; Jakobsen, H. J. Satellite Transitions in MAS NMR Spectra of Quadrupolar Nuclei. *Journal of Magnetic Resonance (1969)* **1991**, *95* (1), 88–117. https://doi.org/10.1016/0022-2364(91)90327-P.
(46) Fleet, M. E.; Muthupari, S. Boron K-Edge XANES of Borate and Borosilicate Minerals. *American Mineralogist* **2000**, *85* (7–8), 1009–1021. https://doi.org/10.2138/am-2000-0716.
(47) Fleet, M. E.; Liu, X. Boron K-Edge XANES of Boron Oxides: Tetrahedral B–O Distances and near-Surface Alteration. *Phys Chem Min* **2001**, *28* (6), 421–427. https://doi.org/10.1007/s002690100173.

"For Table of Contents Only”

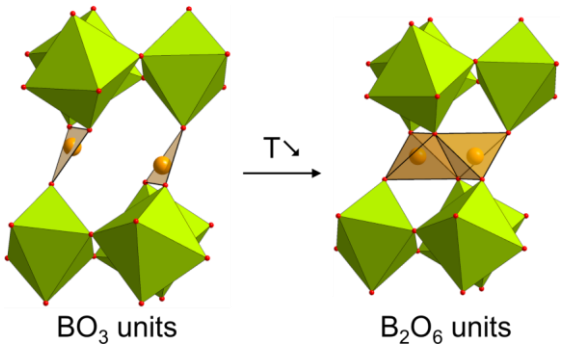

Upon temperature lowering, the $K_3Sb_4BO_{13}$ compound undergoes a phase transition which results in the transformation of every pair of head to tail BO_3 units into one B_2O_6 unit, featuring the edge-sharing BO_4 tetrahedra, extremely rare in the borate chemistry. The $K_3Sb_4BO_{13}$ forms, below and above the phase transition temperature, are characterized by single crystal X-Ray diffraction, as well as Raman, ^{11}B MAS-NMR and B *K*-edge EELS spectroscopies.